# Quantification of $^{11}$C-Laniquidar Kinetics in the Brain

Femke E. Froklage[1,2], Ronald Boellaard[3], Esther Bakker[3], N. Harry Hendrikse[3,4], Jaap C. Reijneveld[2], Robert C. Schuit[3], Albert D. Windhorst[3], Patrick Schober[5], Bart N.M. van Berckel[3], Adriaan A. Lammertsma[3], and Andrey Postnov[3]

*[1]Department of Neurology, Stichting Epilepsie Instellingen Nederland (SEIN), Heemstede, The Netherlands; [2]Department of Neurology, VU University Medical Center, Amsterdam, The Netherlands; [3]Department of Radiology and Nuclear Medicine, VU University Medical Center, Amsterdam, The Netherlands; [4]Department of Clinical Pharmacology and Pharmacy, VU University Medical Center, Amsterdam, The Netherlands; and [5]Department of Anesthesiology, VU University Medical Center, Amsterdam, The Netherlands*

Overexpression of the multidrug efflux transport P-glycoprotein may play an important role in pharmacoresistance. $^{11}$C-laniquidar is a newly developed tracer of P-glycoprotein expression. The aim of this study was to develop a pharmacokinetic model for quantification of $^{11}$C-laniquidar uptake and to assess its test–retest variability. **Methods:** Two (test–retest) dynamic $^{11}$C-laniquidar PET scans were obtained in 8 healthy subjects. Plasma input functions were obtained using online arterial blood sampling with metabolite corrections derived from manual samples. Coregistered T1 MR images were used for region-of-interest definition. Time–activity curves were analyzed using various plasma input compartmental models. **Results:** $^{11}$C-laniquidar was metabolized rapidly, with a parent plasma fraction of 50% at 10 min after tracer injection. In addition, the first-pass extraction of $^{11}$C-laniquidar was low. $^{11}$C-laniquidar time–activity curves were best fitted to an irreversible single-tissue compartment (1T1K) model using conventional models. Nevertheless, significantly better fits were obtained using 2 parallel single-tissue compartments, one for parent tracer and the other for labeled metabolites (dual-input model). Robust $K_1$ results were also obtained by fitting the first 5 min of PET data to the 1T1K model, at least when 60-min plasma input data were used. For both models, the test–retest variability of $^{11}$C-laniquidar rate constant for transfer from arterial plasma to tissue ($K_1$) was approximately 19%. **Conclusion:** The accurate quantification of $^{11}$C-laniquidar kinetics in the brain is hampered by its fast metabolism and the likelihood that labeled metabolites enter the brain. Best fits for the entire 60 min of data were obtained using a dual-input model, accounting for uptake of $^{11}$C-laniquidar and its labeled metabolites. Alternatively, $K_1$ could be obtained from a 5-min scan using a standard 1T1K model. In both cases, the test–retest variability of $K_1$ was approximately 19%.

**Key Words:** P-glycoprotein; modeling; positron emission tomography; blood-brain barrier; test–retest

**J Nucl Med 2015; 56:1730–1735**
DOI: 10.2967/jnumed.115.157586

In many central nervous system disorders, patients respond poorly to drug treatment. For example, 30% of all patients with epilepsy are therapy-resistant (*1*). In epilepsy, pharmacoresistance is attributed, at least in part, to the upregulation of multidrug efflux transporters at the blood–brain barrier, including P-glycoprotein (*2*). These efflux transporters transport substrates (including many central nervous system drugs) back into the circulation, thereby restricting their build-up in the brain (*2*). Consequently, cerebral drug levels may be too low for a therapeutic effect.

PET is a noninvasive molecular imaging technique that has the potential to measure distribution and function of P-glycoprotein in the human brain. Several P-glycoprotein tracers have been proposed, but in practice only (*R*)-$^{11}$C-verapamil and $^{11}$C-*N*-desmethyl-loperamide have been used to assess P-glycoprotein function (*3–7*). Because both ligands are substrates of P-glycoprotein, their concentration in the brain is low. In the case of overexpression of P-glycoprotein, cerebral concentrations will be reduced even further. Consequently, noise levels will increase and accurate measurements of P-glycoprotein overexpression will become difficult. At present, the only option to assess P-glycoprotein overexpression is to obtain 2 scans in the same subject, one before and the other after P-glycoprotein inhibition (*5*), but the statistical limitations mentioned above remain.

Measurement of P-glycoprotein expression should be easier using a P-glycoprotein inhibitor rather than a P-glycoprotein substrate tracer, because such an antagonist should bind in a dose-dependent manner to P-glycoprotein—that is, overexpression of P-glycoprotein should result in an increased signal. Third-generation P-glycoprotein inhibitors, such as laniquidar, elacridar, and tariquidar, have recently been labeled with $^{11}$C (*8–10*). Unfortunately, initial studies on uptake of $^{11}$C-laniquidar in the rat brain have been inconclusive (*10*), and to date only a biodistribution study has been performed in humans (*11*). The purposes of the present study were to develop a tracer kinetic model for quantification of $^{11}$C-laniquidar kinetics in the brain of healthy volunteers and to define test–retest variability of the most appropriate outcome measure.

## MATERIALS AND METHODS

### Subjects

Healthy subject recruitment, screening, and inclusion and exclusion criteria were identical to those described previously (*12*). The study was approved by the Medical Ethics Review Committee of the VU University Medical Center, and before inclusion all subjects gave written informed consent after a complete written and verbal description of the study.

### MR Imaging

All subjects underwent structural MR imaging using a 3-T MR imaging scanner (Signa HDXt; GE Healthcare) according to a standard

Received Mar. 16, 2015; revision accepted Aug. 3, 2015.
For correspondence or reprints contact: Femke E. Froklage, Department of Radiotherapy, PK-1X166, VU University Medical Center, P.O. Box 7057, 1007 MB Amsterdam, The Netherlands.
E-mail: f.froklage@vumc.nl
Published online Aug. 20, 2015.

protocol including T1-weighted 3-dimensional magnetization-prepared rapid acquisition gradient-echo images covering the whole brain, axial fluid-attenuated inversion recovery images, and T2 axial images. Coronal magnetization-prepared rapid acquisition gradient-echo images were used for coregistration and for region-of-interest (ROI) definition.

### Synthesis of $^{11}$C-Laniquidar

$^{11}$C-laniquidar was synthesized as described previously (*10,11*) in a good-manufacturing-practice-compliant manner. $^{11}$C-laniquidar was obtained as a sterile and pyrogen-free solution for intravenous injection in a yield of 800–1,700 MBq, a specific activity of 20–135 GBq·μmol$^{-1}$, and a radiochemical purity greater than 98%. Polysorbate-80 (2.5% w/v) was added to dissolve $^{11}$C-laniquidar in a solution of 10% (v/v) ethanol in 7 mM sodiumphosphate buffer (pH 5.5) in saline.

### PET Data Acquisition

In principle, participants underwent 2 identical PET scans on the same day. If this was not possible, the maximum interval between both scans was 1 mo. PET scans were obtained under standard resting conditions using an ECAT EXACT HR+ scanner (Siemens/CTI) (*13*). All subjects received both indwelling arterial (radial artery) and venous cannulas that were used for arterial blood sampling and tracer injection, respectively. After cannulation, patients were transferred to the scanner room and positioned such that the head was in the center of both the axial and the transaxial fields of view of the scanner. The head was immobilized to reduce movement artifacts and, using laser beams, positioned and checked for movement during scanning.

First, a 10-min transmission scan was obtained in 2-dimensional acquisition mode using 3 retractable rotating line sources. This scan was used to correct the subsequent emission scan for photon attenuation. After this transmission scan, an intravenous injection of approximately 370 MBq of $^{11}$C-laniquidar was administered, simultaneously with the start of a dynamic emission scan in 3-dimensional acquisition mode. $^{11}$C-laniquidar (in a 2.5-mL vial) was injected at a rate of 0.8 mL·s$^{-1}$ using an infusion pump (Med-Rad), followed by a flush of 42 mL of saline at a rate of 2.0 mL·s$^{-1}$. The emission scan consisted of 24 frames with increasing frame duration ($1 \times 15$, $3 \times 5$, $3 \times 10$, $2 \times 30$, $3 \times 60$, $2 \times 150$, and $10 \times 300$ s) and a total scan duration of 60 min. During the emission scan, arterial blood was withdrawn continuously at a rate of 5 mL·min$^{-1}$ for the first 5 min and 2.5 mL·min$^{-1}$ thereafter using an automatic online blood sampler (Veenstra Instruments) (*14*). Continuous withdrawal was interrupted briefly at 2.5, 5, 10, 20, 30, 40, and 60 min after tracer injection for manual collection of 10-mL blood samples. After each manual sample, the arterial line was flushed with a heparinized saline solution. After a resting period of at least 3 h to allow for decay of $^{11}$C, the scanning sequence was repeated in exactly the same manner.

Plasma and whole-blood activity concentrations of the manual samples were measured using a Wallac Wizard 1480 gamma counter, which was cross-calibrated against the PET scanner. Manual blood samples were also used to determine plasma fractions of $^{11}$C-laniquidar and its radiolabeled metabolites. Metabolite analysis was performed using solid-phase extraction. In brief, 1 mL of plasma was diluted with 2 mL of acidified water (10 μL 6 M HCl) and passed over an activated SepPak tC18 (Waters). After being washed with 3 mL of water, the column was eluted with 3 mL of methanol. The first 2 fractions consisted of polar metabolites. Further analysis of the nonpolar methanol fraction showed only 1 compound (i.e., $^{11}$C-laniquidar).

### PET Data Analysis

PET sinograms were corrected for dead time, scatter, randoms, decay, and tissue attenuation. Images were reconstructed using a standard filtered backprojection algorithm and an image matrix size of $256 \times 256 \times 63$, resulting in a voxel size of $1.2 \times 1.2 \times 2.4$ mm and a spatial resolution of approximately 7 mm in the center of the field of view. Next, PET and MR images were spatially coregistered using a mutual information registration algorithm incorporated within Vinci software (Max Planck Institute) (*15*). Structural T1 MR images were segmented in probability maps of gray matter, white matter, and cerebrospinal fluid using statistical parametric mapping (SPM5; Wellcome Trust Centre for Neuroimaging) (*16*). Thirty-eight ROIs were defined on the segmented MR image using a probabilistic template as implemented within PVElab software (*17*). Gray matter voxels that were not included in any of these spatially localized ROIs were assigned to a rest-of-gray-matter ROI, so that an additional analysis for total gray matter could be performed. All ROIs were mapped onto the coregistered dynamic PET images, thus generating corresponding time–activity curves.

The following ROIs were used for further analysis: frontal (volume-weighted average of orbital frontal, medial inferior frontal, and superior frontal), parietal, temporal (volume-weighted average of superior temporal and medial inferior temporal), medial temporal lobe (volume-weighted average of hippocampus and enthorinal), posterior cingulate and anterior cingulate, occipital, and cerebellum. Finally, a global brain ROI was defined as the volume-weighted average of all 38 original gray matter ROIs.

### Kinetic Analysis

Whole-blood radioactivity concentrations derived from the manual arterial blood samples (excluding the 2.5-min-after-injection sample) were used to individually calibrate each online (whole-blood) sampler curve. Next, this calibrated whole-blood curve was transferred into a total plasma curve by multiplying it with a 3-exponential function that was fitted to the plasma–to–whole-blood ratios derived from all manual samples. Finally, the resulting total plasma curve was multiplied with a Hill function fitted to the time course of the parent fractions (*18*), resulting in a metabolite-corrected arterial plasma input function.

Tissue time–activity curves were fitted to irreversible and reversible 1- (1T1K: rate constant for transfer from arterial plasma to tissue [$K_1$]; 1T2K: $K_1$, $k_2$, which are in- and efflux rate constants, respectively) and

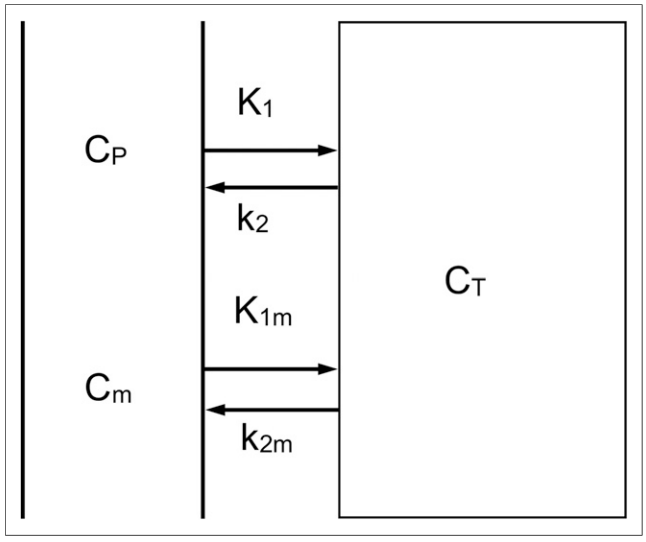


**FIGURE 1.** Dual-input model. $C_P$ and $C_m$ represent plasma concentrations of parent tracer and labeled metabolites, respectively, and $C_T$ the concentration in tissue; $K_1$ and $k_2$ represent influx and efflux rate constants for parent tracer, respectively, and $K_{1m}$ and $k_{2m}$ influx and efflux rate constants for labeled metabolites, respectively.

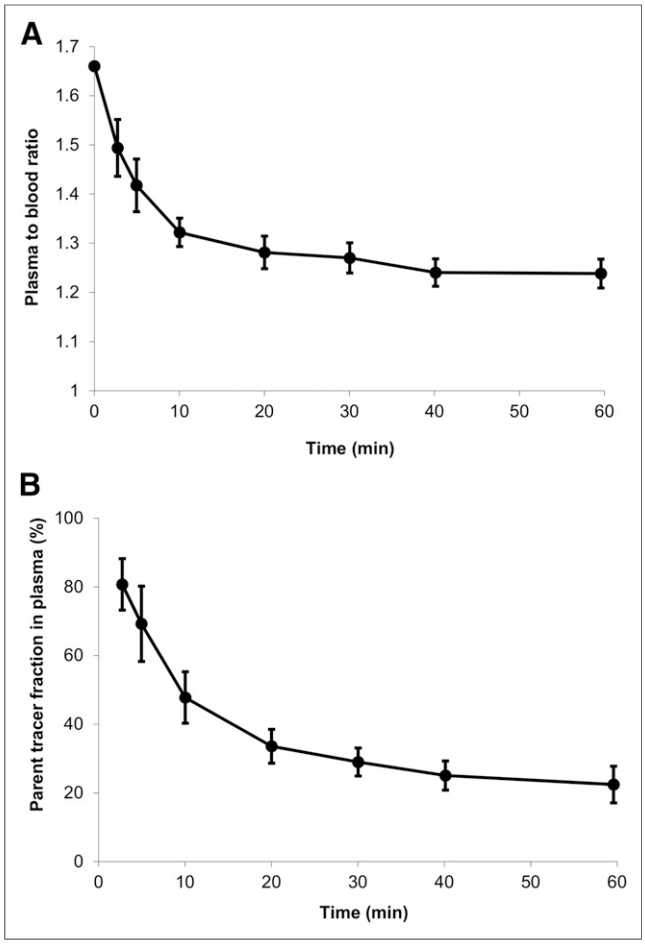


**FIGURE 2.** Plasma–to–whole-blood ratio (A) and parent tracer fraction in plasma (B) derived from manually collected blood samples as function of time averaged over all scans (vertical lines indicate SDs).

2- (2T3K: $K_1$, $k_2$, $k_3$; 2T4K: $K_1$, $k_2$, $k_3$, $k_4$; these are all rate constants for transfer between tissue compartments) tissue-compartment models using the metabolite-corrected plasma curve as input function. In all these models, blood volume $V_B$ was included as a fit parameter (using the calibrated whole-blood curve as its input function). In addition, a dual-input model with parallel parent and metabolite plasma input functions (Fig. 1) was investigated. The Akaike information criterion was used to select the best model (*19*). Finally, the possibility of reducing scan duration was investigated by removing an increasing number of frames from the end of each scan. Resulting outcome parameters were compared with those obtained from the full scan using correlation analysis and Bland–Altman plots (*20*).

### Statistical Analysis

Test–retest variability was calculated as the absolute difference between test and retest scan values divided by their mean (*12*). *P* values for assessing differences in characteristics between test and retest scans were obtained using nonparametric Wilcoxon signed-rank tests. Data are presented as mean ± SD, unless otherwise stated.

## RESULTS

Twelve healthy subjects were included (6 men; mean age, 32 y; age range, 19–63 y). As a result of technical problems (occlusion arterial line, tracer production failure), test–retest data of 8 subjects (5 men; mean age, 30 y; age range, 19–43 y) were available for analysis. Seven underwent 2 identical PET scans on the same day, and in 1 subject the second scan was obtained 1 mo after the first.

### Blood Analysis

Plasma–to–whole-blood ratios and average parent fractions in plasma derived from the manual blood samples are shown in Figure 2. The plasma–to–whole-blood ratio decreased from 1.66 at the beginning of the scan to 1.23 at 60 min after tracer injection (Fig. 2A). The metabolism of $^{11}$C-laniquidar was relatively fast, with only 50% and 20% of parent tracer left at 10 and 60 min after tracer injection, respectively (Fig. 2B). No nonpolar metabolites were detected.

### Kinetic Analysis

Kinetic analysis ($n$ = 8) of $^{11}$C-laniquidar was complicated by low cerebral uptake and fast plasma clearance. Typical images at different time points after tracer injection are shown in Figure 3. Cerebral $^{11}$C-laniquidar uptake slowly increased over time (Fig. 4), suggesting irreversible or at least very slow binding. According to the Akaike information criterion, the 1T1K model was preferred over all standard plasma input models for 15 of the 16 scans, primarily because $k_2$ was close to zero, and therefore additional kinetic parameters did not improve the quality of the fits.

Although the 1T1K model provided the best fits to the 60-min time–activity curves, there were systematic differences between fits and measured data at early time points (Fig. 4A). Taking into account that radiolabeled metabolites of $^{11}$C-laniquidar, probably $^{11}$C-methanol resulting from hydrolysis of the methyl ester, may enter the brain, a dual-input model (Fig. 1) was evaluated. This dual-input model, indicating reversible tracer kinetics, provided better fits (Fig. 4B) than the standard 1T1K model (14 of the 16 scans provided lower

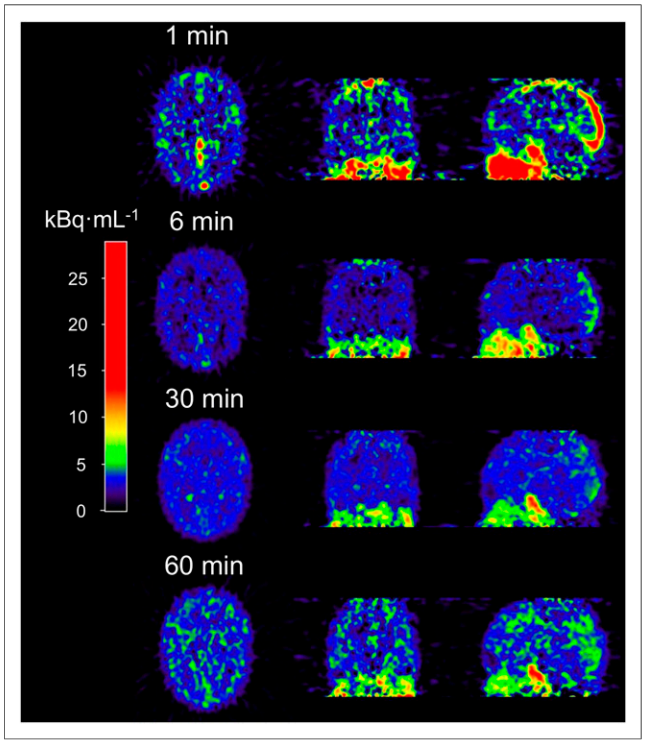


**FIGURE 3.** Example of cerebral $^{11}$C-laniquidar images (kBq·mL$^{-1}$) showing increased uptake at later times.

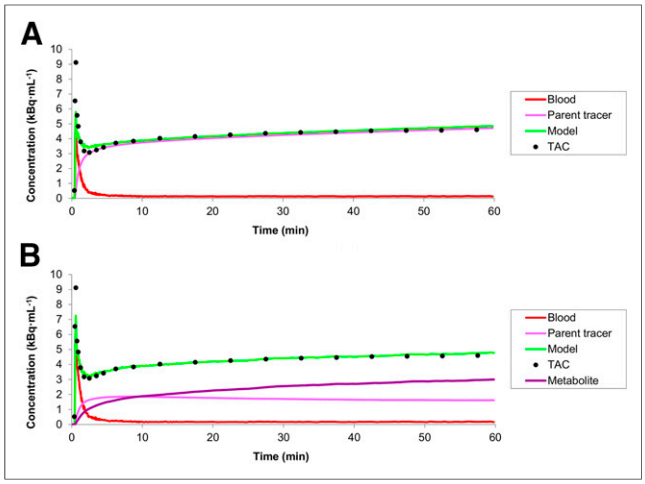


**FIGURE 4.** Example of fits to total gray matter $^{11}$C-laniquidar time–activity curves (TAC) using standard irreversible single-tissue-compartment model (A) and reversible dual-input model (B).

Akaike information criterion scores). Unfortunately, fitted values for the volumes of distribution ($V_T$s) with this dual-input model showed poor precision, especially for parent $^{11}$C-laniquidar (Table 1). In contrast, fitted values for parent $K_1$ showed good precision (Table 1) and were close to those of the 1T1K model.

Given the simplicity of the 1T1K model, it seemed likely that scan duration could be shortened to simplify the scanning procedure, possibly enabling more patients to be scanned from a single tracer production. Several scan durations were investigated, indicating that a 5-min scan was sufficient for stable estimates of $K_1$. Global brain $K_1$ values were approximately 10% lower when only the first 5 rather than the full 60 min of scan data were used. This difference of approximately 10% was also observed at a regional level, with the exception of small ROIs (medial temporal lobe and anterior cingulate, both $< 15$ mL) in which on average up to 17% differences were observed. Global brain $K_1$ values for test and retest were $0.019 \pm 0.002$ and $0.021 \pm 0.005$, respectively, for 60-min tissue data (1T1K model). Corresponding values for just the first 5 min of data were $0.017 \pm 0.002$ and $0.019 \pm 0.005$, respectively. Figure 5 shows the relationship between $K_1$ values derived from 5 and 60 min of tissue data.

### Test–Retest Variability

There were no differences between baseline and retest scans with respect to injected dose ($347 \pm 59$ and $366 \pm 27$ MBq, respectively; $P = 0.48$) and specific activity ($46 \pm 26$ and $71 \pm 47$ GBq·μmol$^{-1}$, respectively; $P = 0.093$) of $^{11}$C-laniquidar. The injected mass of laniquidar, however, was significantly different between baseline and retest scans ($11.35 \pm 4.42$ and $8.34 \pm 3.40$ nmol, respectively; $P = 0.036$), although the difference between test and retest scans was small, compared with the range of masses in either test or retest conditions.

Global brain test–retest variability of fitted $^{11}$C-laniquidar $K_1$ values was 17.7 ± 15.0 (1T1K model), 19.6 ± 13.5 (1T1K model for first 5 min of tissue data), and 19.8 ± 12.7 (dual-input model). This variability was similar at the regional level when the 1T1K model was applied. However, regional fits using the dual-input model were unstable. Table 1 shows global brain test and retest values of fitted $^{11}$C-laniquidar rate constants and $V_T$ values (dual-input model).

## DISCUSSION

This is the first study, to our knowledge, in which kinetics and uptake of the third-generation P-glycoprotein inhibitor $^{11}$C-laniquidar in the human brain were investigated. Several tracer kinetic models were assessed, but given the fact that $k_2$ was close to zero, the best model was a single-tissue-compartment model with a single parameter ($K_1$) for which 5 min of data collection was sufficient. This reduced scanning time was investigated, as it is patient friendly, and in principle several patients could be scanned using a single $^{11}$C-laniquidar production. Clearly, for reliable estimation of $K_1$, online continuous blood sampling is essential, as an arterial input function with high temporal resolution is needed. However, $K_1$ itself has limitations as a measure of P-glycoprotein expression, as in general $K_1$ is flow-dependent, and even in the same subject day-to-day variations in cerebral blood flow do exist (*21*). In the case of $^{11}$C-laniquidar, however, $K_1$ not necessarily is the product of cerebral blood flow and extraction fraction, as its main target is located on the capillary wall. Probably $K_1$ represents a combination of P-glycoprotein expression and affinity for P-glycoprotein and possibly perfusion. Studies using combined $^{15}$O-water and $^{11}$C-laniquidar scans will be needed to determine the role of perfusion. Theoretically, a single-tissue-compartment model with $k_2 = 0$ would be consistent with an irreversible inhibitor of P-glycoprotein. To conclusively determine whether $^{11}$C-laniquidar indeed acts as an inhibitor rather than as a substrate tracer in humans needs to be derived from future blocking studies.

For the 1T1K model, $K_1$ values reduced by about 10% when only the first 5 min of tissue data were used for analysis, indicating that later time points still affected $K_1$. One possible explanation could be an increasing effect of (uptake of) radiolabeled metabolites with increasing scanning duration, Nevertheless, the correlation between $K_1$ values derived from 5- and 60-min datasets was good (Fig. 5). The analysis using 5 min of tissue data was performed using the entire plasma curve (60 min). To shorten study duration in future studies, the acquisition time of plasma data should also be shortened. Unfortunately, the present study protocol was not optimized for 5-min acquisition of plasma data. Nevertheless,

**TABLE 1**
Kinetic Parameters of $^{11}$C-Laniquidar Obtained for Global Brain Using Dual-Input Model

| Parameter | Test | Retest |
|---|---|---|
| $K_1$ | 0.016 ± 0.003 | 0.017 ± 0.003 |
| $k_2$ | 0.015 ± 0.016 | 0.015 ± 0.015 |
| $K_{1m}$ | 0.055 ± 0.035 | 0.053 ± 0.031 |
| $k_{2m}$ | 0.10 ± 0.08 | 0.12 ± 0.07 |
| $V_T$ | 1.84 ± 1.07 | 2.14 ± 1.58 |
| $V_{Tm}$ | 0.60 ± 0.23 | 0.48 ± 0.13 |
| $V_B$ | 0.056 ± 0.013 | 0.050 ± 0.009 |

Data are presented as mean ± SD across all subjects. $K_1$ (mL·cm$^{-3}$·min$^{-1}$) and $k_2$ (min$^{-1}$) are influx and efflux rate constants for parent tracer, respectively; $K_{1m}$ (mL·cm$^{-3}$·min$^{-1}$) and $k_{2m}$ (min$^{-1}$) are influx and efflux rate constants for labeled metabolites, respectively; $V_T$ and $V_{Tm}$ are distribution volume for parent tracer and for labeled metabolites, respectively; and $V_B$ is fractional blood volume.

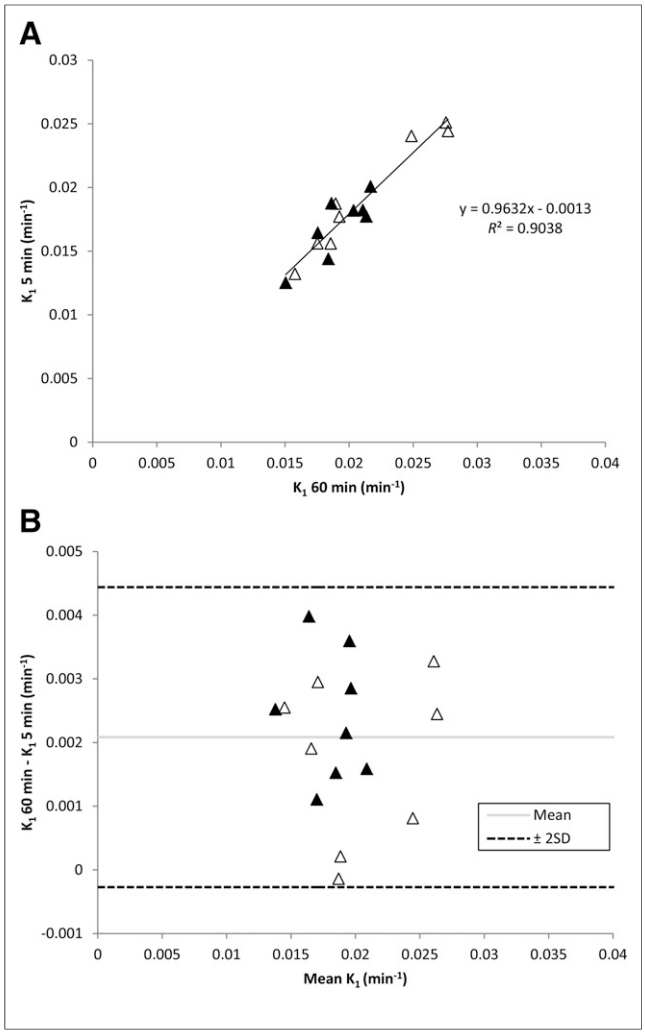


**FIGURE 5.** Correlation between 5- and 60-min scan duration for $K_1$ (A) and Bland–Altman plot of global $K_1$ values for 5- and 60-min scan duration (B). ▲ = test data; △ = retest data.

the 5-min tissue data were reanalyzed using only information from the first 5 min of plasma data. Resulting $K_1$ values were, on average, essentially the same as those derived from the analysis using all plasma data, although there was somewhat more spread in individual values. This indicates that, after optimizing, it should be feasible to shorten acquisition of plasma data to 5 min.

As mentioned above, metabolism of $^{11}$C-laniquidar was fast, with only 50% and 20% of intact $^{11}$C-laniquidar left at 10 and 60 min after tracer injection, respectively. This metabolic profile of $^{11}$C-laniquidar in humans is different from that in rats, for which 68% of parent $^{11}$C-laniquidar was still present at 30 min after tracer injection (*10*). The present findings, however, were not completely unexpected, as laniquidar is radiolabeled at the ester moiety, and methyl esters are known to be unstable in vivo (*10*) due to esterases in the blood. In fact, it is not clear why $^{11}$C-laniquidar metabolism in the rat is so low. A potential radiolabeled metabolite of $^{11}$C-laniquidar is $^{11}$C-methanol, which would result from hydrolysis of the methyl ester. Because this metabolite is likely to enter the brain and plasma levels of labeled metabolites were high, a dual-input model was evaluated. This model, accounting for uptake of both $^{11}$C-laniquidar and its labeled metabolites, provided good fits with reversible kinetics. Unfortunately, fitted parameters, especially $V_T$, suffered from high variability (Table 1).

Although there are limitations in the use of $K_1$ for assessing P-glycoprotein expression in the case of reversible inhibitors, the use of $V_T$ for reversible inhibitors also is not clear-cut. $V_T$ reflects the ratio of $K_1$ and $k_2$, which traditionally reflect rate constants for transport into and out of the brain, respectively. For P-glycoprotein, being located at the capillary wall, $V_T$ would only reflect P-glycoprotein expression if $K_1$ and $k_2$ reflect P-glycoprotein on and off rates, respectively. If the tracer also enters brain tissue, both these parameters will represent a mixture of binding characteristics to P-glycoprotein in the capillary wall, and transport in and out of the brain, complicating interpretation of measured $V_T$ values.

It has been suggested that, at tracer doses, laniquidar may act as a P-glycoprotein substrate rather than as a P-glycoprotein inhibitor, because cerebral $^{11}$C-laniquidar uptake was significantly higher in the presence of dose of 60 mg·kg$^{-1}$ of laniquidar in wild-type mice (*22*). Furthermore, significantly increased cerebral uptake of $^{11}$C-laniquidar has been observed in rats pretreated with the P-glycoprotein inhibitor cyclosporine A (*10*). Being a P-glycoprotein substrate would provide a plausible explanation for low cerebral uptake in the present study. Another explanation for low cerebral $^{11}$C-laniquidar uptake could be that interaction between $^{11}$C-laniquidar and P-glycoprotein takes place at the blood–brain barrier, which only constitutes 0.1% of the total brain weight (*23,24*). In other words, the physical space for tracer accumulation is limited, compared with that of a tracer that enters the brain. Recently it has been postulated that not only very low P-glycoprotein density in the brain but also high protein binding of highly lipophilic P-glycoprotein inhibitors such as laniquidar, which in turn results in locally reduced plasma concentrations of the tracer of approximately 0.05%, account for the low cerebral $^{11}$C-laniquidar uptake (*25*).

Unfortunately, in the present study a significant difference in injected mass of laniquidar between test and retest scans was observed. Nevertheless, specific activity was 20 GBq·μmol$^{-1}$ or higher, and therefore no pharmacologic effects would be expected. In addition, test–retest variability for both dual-input and 1T1K models was approximately 19% and no significant differences in $K_1$ between test and retest $^{11}$C-laniquidar scans were found. Thus, the pharmacologic effect (if any) is negligible compared with test–retest variability.

## CONCLUSION

Accurate quantification of $^{11}$C-laniquidar kinetics is hampered by its fast metabolism and the likelihood that labeled metabolites enter the brain. For the 60-min scan interval, best fits were obtained using a kinetic model consisting of 2 parallel single-tissue-compartment models, one for parent $^{11}$C-laniquidar and the other for labeled metabolites. A potential alternative could be the use of a single-tissue-compartment model applied to the first 5 min of data, which provided $K_1$ values similar to the dual-input model. Reproducibility of $^{11}$C-laniquidar $K_1$ values derived from both models was approximately 19%.

## DISCLOSURE

The costs of publication of this article were defrayed in part by the payment of page charges. Therefore, and solely to indicate this fact, this article is hereby marked "advertisement" in accordance with 18 USC section 1734. The research leading to these results has received funding from the European Community's Seventh Framework Program (FP7/2007-2013) under grant agreement no. 201380. Johnson & Johnson Beerse Belgium is acknowledged for their kind gift of laniquidar. No other potential conflict of interest relevant to this article was reported.

## ACKNOWLEDGMENTS

We thank our colleagues for acquisition of MRI and PET data and for tracer production.

## REFERENCES

1. Kwan P, Brodie MJ. Early identification of refractory epilepsy. *N Engl J Med.* 2000;342:314–319.
2. Löscher W. Animal models of drug-resistant epilepsy. *Novartis Found Symp.* 2002;243:149–159.
3. Bauer M, Karch R, Neumann F, et al. Assessment of regional differences in tariquidar-induced P-glycoprotein modulation at the human blood-brain barrier. *J Cereb Blood Flow Metab.* 2010;30:510–515.
4. Kortekaas R, Leenders KL, van Oostrom JC, et al. Blood-brain barrier dysfunction in parkinsonian midbrain in vivo. *Ann Neurol.* 2005;57:176–179.
5. Kreisl WC, Liow JS, Kimura N, et al. P-glycoprotein function at the blood-brain barrier in humans can be quantified with the substrate radiotracer $^{11}$C-*N*-desmethyl-loperamide. *J Nucl Med.* 2010;51:559–566.
6. Sasongko L, Link JM, Muzi M, et al. Imaging P-glycoprotein transport activity at the human blood-brain barrier with positron emission tomography. *Clin Pharmacol Ther.* 2005;77:503–514.
7. Toornvliet R, van Berckel BN, Luurtsema G, et al. Effect of age on functional P-glycoprotein in the blood-brain barrier measured by use of (*R*)-[$^{11}$C] verapamil and positron emission tomography. *Clin Pharmacol Ther.* 2006;79: 540–548.
8. Bauer F, Kuntner C, Bankstahl JP, et al. Synthesis and in vivo evaluation of [$^{11}$C]tariquidar, a positron emission tomography radiotracer based on a third-generation P-glycoprotein inhibitor. *Bioorg Med Chem.* 2010;18: 5489–5497.
9. Dörner B, Kuntner C, Bankstahl JP, et al. Synthesis and small-animal positron emission tomography evaluation of [$^{11}$C]-elacridar as a radiotracer to assess the distribution of P-glycoprotein at the blood-brain barrier. *J Med Chem.* 2009;52: 6073–6082.
10. Luurtsema G, Schuit RC, Klok RP, et al. Evaluation of [$^{11}$C]laniquidar as a tracer of P-glycoprotein: radiosynthesis and biodistribution in rats. *Nucl Med Biol.* 2009;36:643–649.
11. Postnov A, Froklage FE, van Lingen A, et al. Radiation dose of the P-glycoprotein tracer $^{11}$C-laniquidar. *J Nucl Med.* 2013;54:2101–2103.
12. van Assema DM, Lubberink M, Boellaard R, et al. Reproducibility of quantitative (R)-[$^{11}$C]verapamil studies. *EJNMMI Res.* 2012;2:1.
13. Brix G, Zaers J, Adam LE, et al. Performance evaluation of a whole-body PET scanner using the NEMA protocol. National Electrical Manufacturers Association. *J Nucl Med.* 1997;38:1614–1623.
14. Boellaard R, van Lingen A, van Balen SC, Hoving BG, Lammertsma AA. Characteristics of a new fully programmable blood sampling device for monitoring blood radioactivity during PET. *Eur J Nucl Med.* 2001;28:81–89.
15. Cizek J, Herholz K, Vollmar S, Schrader R, Klein J, Heiss WD. Fast and robust registration of PET and MR images of human brain. *Neuroimage.* 2004;22:434–442.
16. Friston KJ, Holmes AP, Worsley KJ, Poline JP, Frith CD, Frackowiak RS. Statistical parametric maps in functional imaging: a general linear approach. *Hum Brain Mapp.* 1994;2:189–210.
17. Svarer C, Madsen K, Hasselbalch SG, et al. MR-based automatic delineation of volumes of interest in human brain PET images using probability maps. *Neuroimage.* 2005;24:969–979.
18. Wu S, Ogden RT, Mann JJ, Parsey RV. Optimal metabolite curve fitting for kinetic modeling of $^{11}$C-WAY-100635. *J Nucl Med.* 2007;48:926–931.
19. Akaike H. A new look at the statistical model identification. *IEEE Trans Automat Cont.* 1974;19:716–723.
20. Bland JM, Altman DG. Statistical methods for assessing agreement between two methods of clinical measurement. *Lancet.* 1986;1:307–310.
21. Bremmer JP, van Berckel BN, Persoon S, et al. Day-to-day test-retest variability of CBF, CMRO2, and OEF measurements using dynamic $^{15}$O PET studies. *Mol Imaging Biol.* 2011;13:759–768.
22. Moerman L, Dumolyn C, Boon P, De VF. The influence of mass of [$^{11}$C]-laniquidar and [$^{11}$C]-N-desmethyl-loperamide on P-glycoprotein blockage at the blood-brain barrier. *Nucl Med Biol.* 2012;39:121–125.
23. Gjedde A, Christensen O. Estimates of Michaelis-Menten constants for the two membranes of the brain endothelium. *J Cereb Blood Flow Metab.* 1984;4:241–249.
24. Pardridge WM, Triguero D, Yang J, Cancilla PA. Comparison of in vitro and in vivo models of drug transcytosis through the blood-brain barrier. *J Pharmacol Exp Ther.* 1990;253:884–891.
25. Kannan P, Pike VW, Halldin C, et al. Factors that limit positron emission tomography imaging of p-glycoprotein density at the blood-brain barrier. *Mol Pharm.* 2013;10:2222–2229.